THE JOURNAL OF BIOLOGICAL CHEMISTRY VOL. 288, NO. 23, pp. 16619–16628, June 7, 2013

Stabilization of the Conductive Conformation of a Voltage-gated K^+ (Kv) Channel

*THE LID MECHANISM**

Received for publication, March 12, 2013, and in revised form, April 15, 2013 Published, JBC Papers in Press, April 22, 2013, DOI 10.1074/jbc.M113.468728

Jose S. Santos[1], **Ruhma Syeda**[1], **and Mauricio Montal**[2]

From the Section of Neurobiology, Division of Biological Sciences, University of California San Diego, La Jolla, California 92093

Background: In voltage-gated K^+ channels, sensor and pore are two structural modules, but their functional coupling remains elusive.
Results: Premature pore closing is bypassed by association of the filter gate with novel open conformation stabilizers.
Conclusion: Prolonged occupancy of cargo at the gate underlies stabilization.
Significance: A gate covered by a lid provides new ways of thinking about gating mechanisms.

Voltage-gated K^+ (Kv) channels are molecular switches that sense membrane potential and in response open to allow K^+ ions to diffuse out of the cell. In these proteins, sensor and pore belong to two distinct structural modules. We previously showed that the pore module alone is a robust yet dynamic structural unit in lipid membranes and that it senses potential and gates open to conduct K^+ with unchanged fidelity. The implication is that the voltage sensitivity of K^+ channels is not solely encoded in the sensor. Given that the coupling between sensor and pore remains elusive, we asked whether it is then possible to convert a pore module characterized by brief openings into a conductor with a prolonged lifetime in the open state. The strategy involves selected probes targeted to the filter gate of the channel aiming to modulate the probability of the channel being open assayed by single channel recordings from the sensorless pore module reconstituted in lipid bilayers. Here we show that the premature closing of the pore is bypassed by association of the filter gate with two novel open conformation stabilizers: an antidepressant and a peptide toxin known to act selectively on Kv channels. Such stabilization of the conductive conformation of the channel is faithfully mimicked by the covalent attachment of fluorescein at a cysteine residue selectively introduced near the filter gate. This modulation prolongs the occupancy of permeant ions at the gate. It is this longer embrace between ion and gate that we conjecture underlies the observed stabilization of the conductive conformation. This study provides a new way of thinking about gating.

Voltage-gated K^+ (Kv)[3] channel subunits assemble into tetramers (1). At the center of the square array, shared by all subunits, is a pore that selects for K^+ ions (2–5). Four voltage sensors, each contributed by a subunit, reside on the periphery of the pore. The role of the voltage sensors is to promote the structural transition between the nonconductive and conductive conformations of the pore at permissive membrane potentials (6, 7). But how does the sensor achieve this?

Pores of Kv channels have two gates: an "activation gate" facing the cytoplasm (8) and a filter gate facing the extracellular milieu (9–11). For the onset of K^+ current, both gates must be in a conductive conformation (12). Functional and structural evidence has shown that opening of the activation gate in Kv channels is strongly coupled to sensor movement: in response to a change in potential, each of the sensors pries open the activation gate in the pore subunit to which it is covalently attached (6, 13, 14). In comparison, the mechanism by which the sensor controls the conformation of the filter gate remains less clear (15–17). An evolutionarily conserved interaction between an activated sensor in one subunit and the filter gate component in an adjacent subunit has been shown to stabilize the filter gate of Shaker, an archetype Kv channel, in a conductive conformation (18). But despite the tugging and massaging by the sensor, the pores of many Kv channels still manage to close while the membrane potential is commanding the channels to be open.

So, if the switch is on, why isn't the machine working? Clearly one or both of the gates of the channel have closed. Decades of investigation into the cause of this decay to a nonconductive conformation has shown that two mechanisms are at hand: a fast "N-type inactivation" resulting from a block of the channel from the cytoplasmic end (19, 20) and a slower "C-type inactivation" arising from a closing of the filter gate (9, 11, 19, 21–24). Based on this evidence, the filter gate was dubbed the "inactivation gate." One salient early clue that the conductive conformation of the filter gate was unstable was the observation that some Kv channels resisted closing when the concentration of a permeant ion at the filter was increased (25–30) or when the filter was blocked (10, 31, 32). A currently held view on the

* This work was supported, in whole or in part, by National Institutes of Health Grant GM-49711 (to M. M.). This work was also supported by University of California San Diego Grant RK-174C (to M. M.).
[1] Both authors contributed equally to this work.
[2] To whom correspondence should be addressed: Section of Neurobiology, Division of Biological Sciences, University of California San Diego, 9500 Gilman Dr., La Jolla, CA 92093. Tel.: 858-534-0931; Fax: 858-822-3763; E-mail: mmontal@ucsd.edu.
[3] The abbreviations used are: Kv, voltage-gated K^+; KvLm, a Kv channel from *Listeria monocytogenes*; FL, full length; PM, pore module; CTX, charybdotoxin; TBA, tetrabutylammonium; DOPA, 1,2-dioleoyl-*sn*-glycero-3-phosphatidic acid; DPhPC,1,2-diphytanoyl-*sn*-glycero-3-phosphocholine; pS, picosiemens.

universal nature of Kv channel C-type inactivation is that the propensity to inactivate is related to the stability of the inactivation gate and that this property is dependent on 1) a strong connectivity network underpinning the filter gate that serves to hold the K^+ binding sites stable even when K^+ is scarce and 2) prolonged permeant ion residence in the filter. Accordingly, gate and permeant ion assume a symbiotic relation that determines the stability of the conductive conformation of the pore (33).

Using KvLm (34, 35), a bacterial Kv channel, as a test case, here we show three novel means by which the premature closure of the inactivation gate can be practically overridden. The three open gate stabilizers identified compensate the low open probability observed in the full-length Kv channel as well as in the KvLm pore only (5, 36). The implication is that in KvLm low open probability is mostly a result of an unstable filter gate. Collectively, we demonstrate that a "rudimentary" sensor containing only three of eight conserved charges previously implicated in the maintenance of voltage sensor fold and voltage-dependent gating is sufficient to produce channel open probabilities higher than its fully endowed Kv channel relatives.

EXPERIMENTAL PROCEDURES

Protein Expression and Purification—KvLm pore module (PM), WT, and mutants as well as KvLm full length (FL) were expressed in *Escherichia coli* XL1-Blue with a C-terminal His tag and purified by Ni^{2+} affinity chromatography as described previously (36) except that all constructs were further purified by size exclusion chromatography on a Superdex 200 10/300 GL (GE Healthcare) column equilibrated with 200 mM KCl, 50 mM HEPES, pH 7.5, 1 mM *n*-dodecyl β-D-maltopyranoside. Single channel mutations were introduced using the QuikChange site-directed mutagenesis kit (Agilent) according to the manufacturer's instructions.

Fluorescein 5-Maleimide Cysteine Labeling—To covalently attach fluorescein 5-maleimide to the E40C PM mutant, a 10-fold molar excess of fluorescein 5-maleimide (AnaSpec) was added to the protein immediately after elution from the Ni^{2+} affinity column and incubated for 2 h at 4 °C in the dark. The coupling reaction was stopped by the addition of a 100-fold molar excess of L-cysteine. The labeled protein was then passed twice through a PD-10 desalting column (GE Healthcare) to remove any uncoupled fluorescein 5-maleimide from the reaction. The fluorescein-labeled mutant was reconstituted immediately thereafter. Analysis by size exclusion chromatography of the PM E40C-fluorescein maleimide complex showed that the labeled PM eluted from size exclusion chromatography at the same elution volume (±0.1 ml) as the unlabeled protein, suggesting that the labeling did not change the oligomeric state of the protein. In addition, the labeled protein migrates on an SDS-PAGE gel as a tetramer as does the WT (36). Calculation of the protein (A_{280}, $\epsilon = 16{,}960\ M^{-1}\ cm^{-1}$) and fluorescein dye ($A_{500}$, $\epsilon = 68{,}000\ M^{-1}\ cm^{-1}$) concentrations suggests that on average only one subunit in the tetrameric channel was labeled.

Liposome Preparation and Protein Reconstitution—Liposomes were composed of 90% (mol %) 1,2-diphytanoyl-*sn*-glycero-3-phosphocholine (DPhPC) and 10% negatively charged lipid 1,2-dioleoyl-*sn*-glycero-3-phosphatidic acid (DOPA) (Avanti Polar Lipids, Alabaster, AL). Liposomes were prepared as described previously (37). For reconstitution, the protein was diluted ~100–300-fold into preformed liposomes to give a final protein concentration of 2–5 μg/ml. The proteoliposomes were incubated on ice for 15 min prior to bilayer recording experiments. Fresh aliquots of liposomes and protein were used for every experiment.

Single Channel Recordings Using Droplet Interface Lipid Bilayers—Single channel currents were recorded from droplet interface bilayers as described (5, 37). Briefly, a 10 × 10 × 4-mm plexiglass chamber was filled with hexadecane (Sigma-Aldrich) containing 1% DPhPC. A 0.2-mm-diameter Ag/AgCl wire electrode (30–40 mm in length) was attached to each of two micromanipulators (NMN-21, Narishige, London, UK). Droplets (~200 nl) were placed with a pipette on each of the electrodes, which had been coated with 3% (w/v) low melt agarose (65 °C). The electrode carrying the droplet with the proteoliposomes in 0.5 M KCl, 10 mM HEPES, pH 7.4 was connected to the grounded end (*cis* side) of the amplifier headstage. The second electrode in a droplet containing liposomes in the same buffer was connected to the working end of the headstage (*trans* side). The chamber, electrodes, and amplifier headstage were enclosed in a Faraday cage. The droplets were incubated in hexadecane containing 1% DPhPC until a monolayer of lipid had formed around them (~5 min). A bilayer spontaneously formed when the two droplets were brought into contact. All the electrical measurements were performed at 22 ± 2 °C in 0.5 M KCl, 10 mM HEPES, pH 7.4 at +150 mV unless otherwise indicated.

Blockers and Modulators—Tetrabutylammonium (TBA) ion (5 mM) and imipramine (100 μM) stocks were made in droplet solution (0.5 M KCl, 10 mM HEPES, pH 7.4) and injected according to the requirement of experiments to final concentrations of 50 and 5 μM, respectively, using a Nano injector (VWR International). Charybdotoxin stock (50 μM) was made in 50 mM KCl, 10 mM HEPES, pH 7.4 and injected to a final concentration of 1 μM. Alternatively, charybdotoxin (CTX) and imipramine were preincubated with proteoliposomes (~15 min) to final concentrations of 1 and 5 μM, respectively, extruded nine times through a 0.1-mm filter (Mini Extruder) prior to droplet formation to ensure homogenous mixing and accessibility of CTX and imipramine to the reconstituted protein. Both methods of introducing CTX and imipramine produced the same results. Iminodibenzyl (in chloroform) was mixed with 10% DOPA, 90% DPhPC (in chloroform). The mixture was dried under a stream of nitrogen and rehydrated in 0.5 M KCl, 10 mM HEPES, pH 7.4. Liposomes containing iminodibenzyl (5 μM) were extruded prior to protein reconstitution.

Single Channel Acquisition and Analyses—Single channel currents were sampled at 20 kHz using an Axon 200B patch clamp amplifier, filtered by using a low pass Bessel filter (80 db/decade) with a corner frequency of 2 kHz, and then digitized with a DigiData 1320 A/D converter (Axon Instruments). All preprocessing and analysis of the single channel records was performed with QuB software. Records of PM and FL in the presence of imipramine or CTX were further filtered to 200–500 Hz. Event detection was performed by time course fitting with the segmental *k*-means algorithm (38). To avoid the detec-

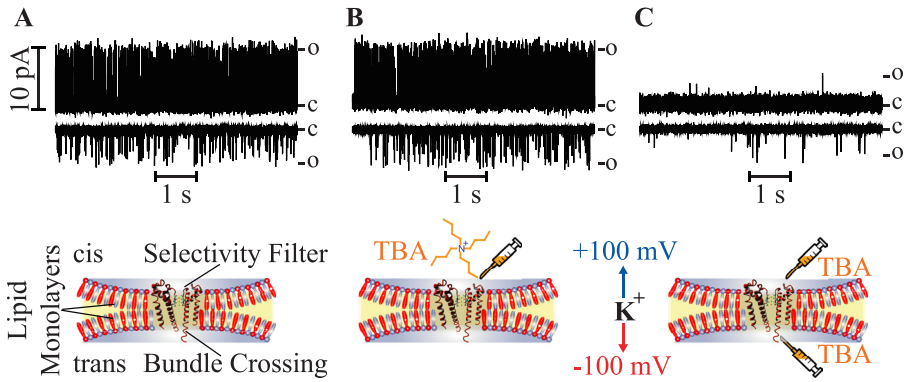

FIGURE 1. **Probing the orientation of KvLm PM in a lipid bilayer using the open channel blocker TBA.** KvLm PM currents recorded in 90% DPhPC, 10% DOPA symmetric bilayers at +100 mV (*top*) and at −100 mV (*bottom*) without TBA (*A*), with 50 μM TBA bathing the filter gate (*B*) and with 50 μM TBA bathing both gates (*C*) are shown. A schematic representation of the PM (*orange*) in a lipid bilayer (*blue contour*) showing the orientation of the channel and the TBA injection site for each panel is shown. DPhPC is depicted in *cyan*, and DOPA is depicted in *red*. The representative recordings shown are selected from a single experiment before and after addition of TBA. *c*, closed; *o*, open.

tion of erroneous events, the receiver dead time (t_d) was set at 300 μs for all records except for PM and FL in the presence of imipramine or CTX; in the indicated cases, t_d was set to 1000–2000 μs. Therefore, transitions shorter than t_d were ignored; transitions longer than t_d were accepted as "events." Single channel conductance was calculated from Gaussian fits to current histograms. Statistical values represent means ± S.E. *n* and *N* denote the number of experiments and number of events, respectively.

Imipramine and Iminodibenzyl Docking—Docking of the ligands imipramine and iminodibenzyl onto the receptor KvLm PM (Protein Data Bank codes 4H33 and 4H37) was performed by AutoDock 4.2 (39) using the default docking parameters supplied with AutoDock in the "examples" subdirectory, and point charges were assigned according to the AMBER03 force field (40) in YASARA (Yasara Biosciences GmbH, Austria). Receptor flexibility is considered by creating a receptor ensemble with five receptor conformations with alternative high scoring solutions of the side-chain rotamer network. Conservation of 4-fold (Protein Data Bank code 4H33) or 2-fold (Protein Data Bank code 4H37) symmetry was not imposed for the ensemble receptor structures. Ligand is allowed full flexibility. Each docking experiment consisted of 500 ligand to receptor docking runs (100 runs per receptor conformation). Docking results usually cluster around certain hot spot conformations, and the complex with the lowest free energy of binding (strongest interaction) in each cluster is saved. The more negative the free energy of binding, the stronger the interaction between ligand and receptor. Importantly, these energies are potential force field energies, and therefore the results cannot be quantitatively compared with experimentally measured free energies of binding. Therefore, these potential force energy values can only be used for comparative evaluation of binding energies calculated under the same force field. Two complexes belong to different clusters if the ligand heavy atom root mean square deviation is larger than 5 Å. All docking experiments were performed at 298 K. Scoring of each receptor-ligand ensemble was performed by AutoDock. The docking surface on the receptor was limited to the extracellularly facing side of the PM. To test the dependence of the docking interaction on the occupancy of the filter gate by K^+, replica docking was tested with three K^+ ions at ion binding positions S2, S3, and S4 in the filter as seen in Protein Data Bank code 4H33, four K^+ ions at positions S1, S2, S3, and S4 as seen in Protein Data Bank code 4H37, and five K^+ ions at positions S0, S1, S2, S3, and S4 in the selectivity filter. To generate the five-K^+ structure, the structure of KcsA (Protein Data Bank code 1K4C (41)) was aligned with that of KvLm PM with four K^+ ions at the filter, and the ion at S0 in Protein Data Bank code 1K4C was transferred to the KvLm structure. The results of all docking experiments are summarized in Table 3.

CTX Docking—Docking of CTX onto the extracellular surface of KvLm PM (Protein Data Bank code 4H33), stripped of all K^+ ions, was achieved by generating a start complex of CTX and KvLm PM and feeding this complex to the RosettaDock server for local protein-protein docking (ROSIE). The starting complex was generated by aligning the KvLm PM structure with that of a KcsA mutant in a complex with CTX (Protein Data Bank code 2A9H (42)) and transferring the CTX protein to the KvLm PM. The RosettaDock server performs a local docking search starting with the initial complex in which both ligand and receptor are allowed some flexibility. In detail, the local perturbation of RosettaDock includes ~±3 Å in the direction between the two proteins, ~8 Å in the directions sliding the proteins relative to each other along their surfaces, ~8° of tilt of the proteins, and a complete 360° spin around the axis between the centers of the two proteins. The server performs 1000 independent simulations from this range of random positions and returns the 10 best scoring complex structures ordered by energy. The two complex structural models shown (see Fig. 3, *D* and *E*) correspond to the highest scoring (Fig. 3*D*) and the fifth highest scoring (Fig. 3*E*) complex models. Noticeably in nine of 10 top scoring models, Glu-40 came within 4 Å of a lysine residue in CTX. These nine models fall into two distinct groups: one in which the lysine of CTX inserts into the filter (similar to Fig. 3*E*) and another where the lysine hovering over the filter bends to contact the Glu-40 side chain (similar to Fig. 3*D*). As a control experiment, the docking experiment was repeated using the KvLm PM mutant E40A. In none of the 10 models did Lys-27 in CTX come close to Ala-40, but in three of these 10 models, Lys-27 in the CTX inserted into the filter in a conformation similar to that shown in Fig. 3*E*.

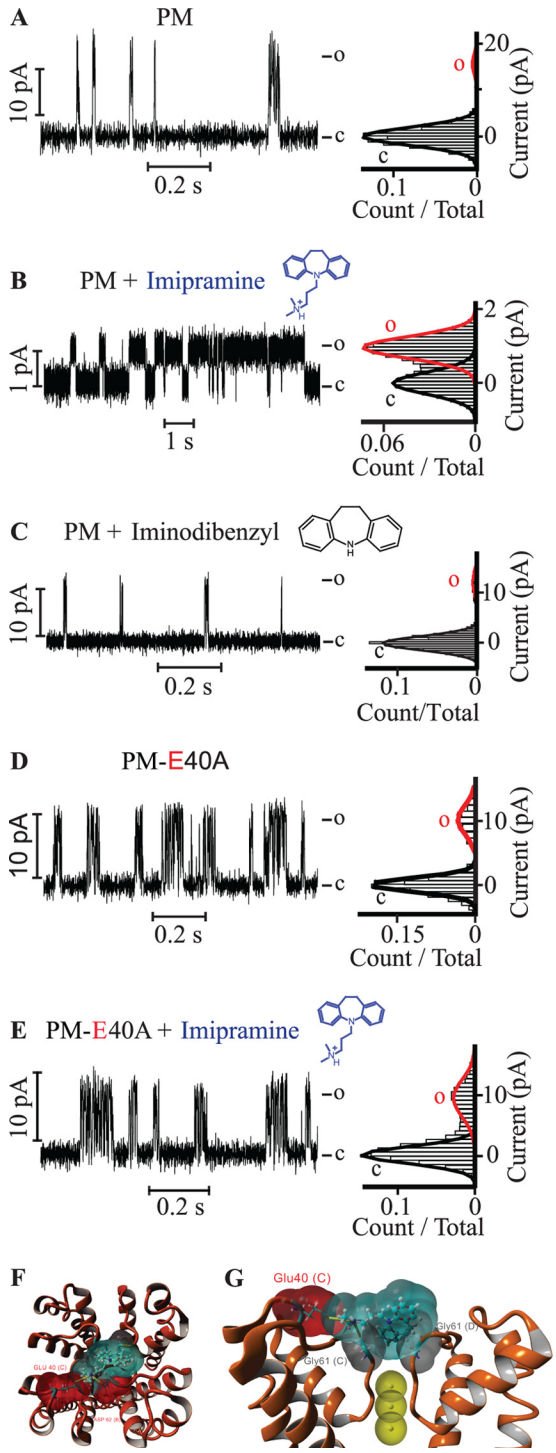

FIGURE 2. **Gating by a charged tricyclic molecule is mediated by a single residue on the PM extracellular surface.** Single channel steady-state current records (*left*) and their corresponding normalized all-point histograms (*right*) of WT KvLm PM (*A* and *B*) and of the KvLm PM E40A mutant (*D* and *E*) in symmetric 10% molar DOPA bilayers with 5 μM imipramine in the *cis* droplet (*B* and *E*) and without (*A* and *D*) are shown. The structure of imipramine, a tricyclic antidepressant, is shown in *blue* above the current recordings in *B* and *E*. *C*, single channel currents recorded (*left*) and the corresponding all-point current histograms (*right*) from PM reconstituted in symmetric DOPA bilayers in the presence of 5 μM iminodibenzyl on the *cis* droplet (filter side). The structure of iminodibenzyl, a structural homologue of imipramine lacking the charged amine group, is shown in *black*. Views from top (*F*) and side (*G*) of the highest scoring model for interaction of imipramine with the filter gate of KvLm PM obtained from docking experiments (see "Experimental Procedures") are shown. The channel PM is depicted in *orange ribbons* (Protein Data Bank code 4H33). The solvent-accessible surfaces of the interacting residues in the PM (Glu-40, Asp-62, and Gly-61) are shown and are color-coded according to charge (*red* for Glu-40 and Asp-62 and *gray* for Gly-61). *Yellow arrows* show interaction sites (<4 Å). Residues are labeled with subunit in *parentheses*. The solvent-accessible surface of imipramine is shown and colored *light blue*. K^+ ions at positions S2, S3, and S4 in the filter are shown as *solid yellow spheres* with their accessible surface depicted. *c*, closed; *o*, open.

Model of Fluorescein Maleimide Coupled to E40C—To generate the model of fluorescein maleimide coupled to E40C (see Fig. 5, *D* and *E*), fluorescein maleimide was first docked onto the extracellular surface of the WT PM using the same methodology used to dock imipramine in YASARA. We took the highest scoring docking model that positioned fluorescein over the filter with the maleimide facing Glu-40, made the E40C mutation *in silico* in all subunits, and moved the fluorescein maleimide only slightly so that the coupling site of the maleimide was within 2.0 Å of the sulfur atom in cysteine and formed a bond. The complex was then energy-minimized to remove any atom clashes and inserted into a dioleoylphosphatidylcholine membrane for a 1-ns molecular dynamics simulation. The average conformation of the complex during the simulation is shown.

RESULTS

Preferential Orientation of a Kv Channel Pore Module in Lipid Bilayers with the Selectivity Filter Accessible from the Extracellular Compartment—To investigate the impact of an interaction between the pore of a Kv channel and the selected probes, the sensorless PM of KvLm was reconstituted in droplet interface bilayers (43) in which both cytoplasmic and extracellular leaflets were of equal composition (symmetric bilayers): 90% molar zwitterionic DPhPC and 10% molar negatively charged DOPA. Channel function was assayed by monitoring the single channel steady-state activity at +100 mV (*top*) and at −100 mV (*bottom*) while bathing both sides of the membrane in 0.5 M KCl (Fig. 1*A*). The PM was observed to open frequently with a single channel conductance (γ) of 107 ± 6 pS and was further characterized by short (~1-ms) sojourns in the open state: PM opening was typically immediately followed by channel closing, thereby defining a low open probability (P_o = 0.020 ± 0.002) (Figs. 1*A* and 2*A*). Sided block by the open channel blocker TBA (8, 44, 45), which is known to access the channel from the intracellular entryway, demonstrated that the PM inserts into the bilayer in predominantly one orientation: the selectivity filter faces the *cis* side (Fig. 1*B*, no TBA block), and the bundle crossing (activation gate) faces the *trans* side (Fig. 1*C*, TBA block).

Stabilization of the Open Conformation of the Channel by a Positively Charged Tricyclic Antidepressant—Given the impact of excess permeant ions on the gating properties of Kv channels (25–30), we looked for positively charged amphipathic molecules that partition into the membrane and change the properties of the lipid bilayer. Imipramine is a tricyclic antidepressant (Fig. 2*B*) that fits the description: it is positively charged, and its insertion into the membrane has been reported to alter the surface charge and the dynamics of the membrane (46). Here we inspected the effect of imipramine on the filter of the PM reconstituted in DOPA bilayers. Addition of 5 μM imipramine to the extracellular milieu was sufficient to depress γ from

TABLE 1
Single channel properties of KvLm PM and FL

Experimental conditions	PM				FL			
	γ	P_o	τ_{open}	$N; n$	γ	P_o	τ_{open}	$N; n$
	pS		*ms*		*pS*		*ms*	
KvLm	107 ± 6	0.020 ± 0.002	1.2 ± 0.2	32,796; 10	70 ± 3	0.07 ± 0.01	2.5 ± 0.2	27,900; 10
KvLm + 5 μM imipramine	10 ± 2	0.67 ± 0.08	180 ± 60	12,598; 5	16 ± 2	0.74 ± 0.08	100 ± 20	19,203; 5
KvLm + 1 μM CTX	15 ± 2	0.7 ± 0.1	200 ± 50	15,642; 5	14 ± 3	0.7 ± 0.1	190 ± 40	9,142; 5

TABLE 2
Single channel properties of KvLm PM WT and Glu-40 mutants

Experimental conditions	γ	P_o	τ_{open}	$N;n$
	pS		*ms*	
PM	107 ± 6	0.020 ± 0.002	1.2 ± 0.2	32,796; 10
PM + iminodibenzyl	65 ± 5	0.010 ± 0.003	1.6 ± 0.3	6,187; 5
PM E40A	78 ± 8	0.07 ± 0.04	1.8 ± 0.4	31,160; 7
PM E40C	80 ± 7	0.06 ± 0.03	1.1 ± 0.3	14,295; 5
PM E40A + imipramine	76 ± 7	0.11 ± 0.05	2.3 ± 0.5	60,856; 5
PM E40A + CTX	75 ± 8	0.11 ± 0.04	3.1 ± 0.6	19,597; 5
PM E40C-fluorescein	7 ± 1	0.74 ± 0.05	120 ± 30	5,400; 4

107 ± 6 to 10 ± 2 pS at the expense of a ~33-fold increase in P_o from 0.020 ± 0.002 to 0.67 ± 0.08 (Fig. 2, *A* and *B*). The increase in P_o was observed to arise primarily from an increase in the mean open time (τ_{open}) within a burst of activity, an ~150-fold increase (Table 1). To resolve the cause of the imipramine effect, we first aimed to separate a direct action on the bilayer from an interaction between imipramine and the PM. We reasoned that if the observed phenotype is a consequence of the high affinity of imipramine for PM then an electrostatic interaction between the positive charge on imipramine and a negative charge on the extracellular surface of the PM may be determinant. In searching for this charge, we discovered that truncation of the charged side chain of Glu-40 in the E40A mutant produced a PM with 80% of the conductance of the WT (78 ± 8 pS in E40A) and WT-like P_o (0.07 ± 0.04 for E40A *versus* 0.020 ± 0.002 for WT) and that was largely insensitive to 5 μM imipramine (Fig. 2, *D* and *E*, and Table 2). From this result, we conclude first that the mutation is responsible only in small part for the decrease in γ and change in P_o and second that the imipramine modulation is a consequence of an interaction between PM and imipramine. Lastly we propose that this interaction occurs between the charged side chain of Glu-40 at the periphery of the extracellular surface of the PM and the charged amine in imipramine. In agreement with this hypothesis, we demonstrate that iminodibenzyl, a compound that retains the tricyclic structure of imipramine but lacks the charged amine group, at up to 50 μM failed to have a significant effect on the conductance and P_o of the PM ($\gamma = 65 \pm 5$ and $P_o = 0.010 \pm 0.003$), thereby directly implicating the charge on imipramine as a determinant (Fig. 2*C* and Table 2). There are two plausible interpretations to the observed dependence of the imipramine effect on Glu-40: either Glu-40 interacts directly with the positive charge on the drug, or alternatively Glu-40 mediates the interaction through an indirect mechanism. To test the direct interaction hypothesis further, we performed *in silico* unbiased docking experiments of imipramine onto the surface of the 3.1-Å-resolution crystal structure of the PM determined in a lipid bilayer (Protein Data Bank code 4H33) (5). In this structure, three K^+ ions are located at ion binding positions S2, S3, and S4 in the filter. Analysis of the docking results predicts that imipramine docks predominantly through the hypothesized interaction of Glu-40 with the drug charge (Figs. 2, *F* and *G*, and 3, *A* and *B*, and Table 3) and surprisingly provides an exciting rationale to be structurally verified for the effect of imipramine on the PM: the anchoring of the charged acyl chain in imipramine at Glu-40 positions an aromatic ring structure at the ion binding site S0 above the ion binding sites in the filter (S1–S4) (47), effectively placing a lid on the extracellular end of the filter gate. In agreement, when the docking experiment was repeated with iminodibenzyl (Fig. 3*D*) or with the S0 site occupied by a K^+ ion (see "Experimental Procedures"), the ligand fails to dock to the filter with high affinity (Fig. 3*C* and Table 3). As predicted by the model, attempts to dock imipramine onto the extracellular surface of the E40A mutant showed a decreased affinity of the mutant PM for imipramine. Based on this analysis, we propose that by opposing the exit of the last ion or water molecule from the filter gate (48–50) at depolarizing potentials the lid stabilizes a conductive conformation of the PM, an effect that

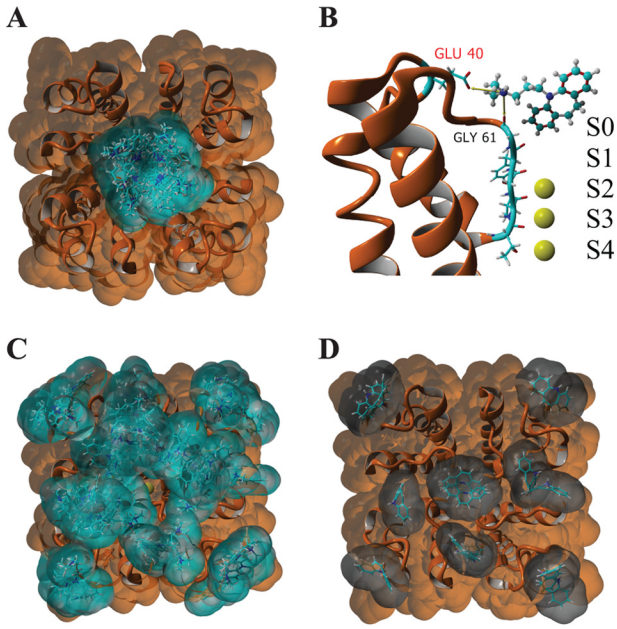

FIGURE 3. **Docking experiments suggest that the experimentally observed strong affinity of the PM for imipramine arises from an interaction between Glu-40 in the PM and the charged amine group in imipramine.** *A*, extracellular view of the solvent-accessible surface of the PM tetramer (colored *orange*; Protein Data Bank code 4H33) with three K^+ ions bound at the filter (S2–S4) showing all imipramine (*cyan* surface) docking clusters. *B*, side view of a single PM subunit with imipramine bound in the docking model with the predicted strongest interaction between ligand and receptor. *S0–S4* denote the K^+ binding sites. *C*, extracellular solvent-accessible surface of the PM tetramer (colored *orange*; Protein Data Bank code 4H37) with five K^+ ions bound at the filter (S0–S4) showing all imipramine docking clusters. *D*, extracellular solvent-accessible surface of the PM tetramer (colored *orange*; Protein Data Bank code 4H33) with three K^+ ions bound at the filter (S2–S4) showing all iminodibenzyl (*gray* surface) docking clusters. The results of all docking experiments are summarized in Table 3.

TABLE 3

Imipramine and iminodibenzyl docking onto the extracellular surface of KvLm PM WT and E40A mutant

NA, not applicable.

Protein Data Bank code	KvLm PM	Ligand	K^+ ions in filter (S0–S4)	ΣBinding free energies of filter clusters	Average binding free energy of filter clusters	Lowest binding free energy of all filter clusters
				kcal/mol	*kcal/mol*	*kcal/mol*
4H33	WT	Imipramine	3 (S2–S4)	−86.26	−6.6 ± 0.5	−7.21
4H37	WT	Imipramine	3 (S2–S4)	−83.59	−6.4 ± 0.4	−6.92
4H37	WT	Imipramine	4 (S1–S4)	−70.56	−6.4 ± 0.3	−6.79
4H37	WT	Imipramine	5 (S0–S4)	NA	NA	NA
4H37	WT	Iminodibenzyl	3 (S2–S4)	−10.94	−5.48 ± 0.02	−5.50
4H37	WT	Iminodibenzyl	3 (S2–S4)	−10.84	−5.43 ± 0.01	−5.44
4H33	E40A	Imipramine	3 (S2–S4)	−77.31	−5.5 ± 0.4	−5.91
4H37	E40A	Imipramine	3 (S2–S4)	−83.85	−6.0 ± 0.3	−6.33

the observed increase in τ_{open} suggests is a result of prolonged residence of K^+ in the filter. To validate this proposal, we showed that the reduced conductance and increased residence in the open state are not due to a markedly constricted activation gate by demonstrating that the PM is blocked by TBA when interacting with imipramine. The implication is that stabilization of the conductive conformation is mediated by appending an amphipathic lid on the extracellular end of the filter gate, thereby prolonging the cargo residence time at the gate.

Charybdotoxin Stabilizes the Conductive Conformation of the Channel through an Interaction with the Filter—CTX is a small protein that blocks the conduction pathway of Shaker with high affinity by inserting a lysine residue (Lys-27) at the S1 ion binding position in the filter, thereby using the charge on its side chain as a surrogate immobile K^+ (51, 52). The identification of residues in Shaker critical for a high affinity interaction with CTX by Miller, MacKinnon, and colleagues (53–57) and others (55) made possible the conversion of a CTX-insensitive KcsA to a mutated, CTX-sensitive KcsA (KcsA-Shaker) (42). An alignment of the protein sequences linking TM5 to TM6 in the PMs of Shaker and KcsA-Shaker with that found in KvLm (Fig. 4*A*) indicates that these critical residues are mostly conserved and suggests that the KvLm PM may be sensitive to CTX. Accordingly, we asked whether CTX modulates the conductive conformation of the filter in KvLm reconstituted in DOPA bilayers. Addition of 1 μM CTX to the extracellular solution efficiently promoted the conversion of a PM with high conductance and low open probability to a low conductance ($\gamma = 15 \pm 2$ pS), long τ_{open} (200 ± 50 ms), and high open probability PM ($P_o = 0.7 \pm 0.1$) (Fig. 4, *B* and *C*), an effect equal within error to that observed for the addition of 5 μM imipramine. Because of the striking similarity between the effects of imipramine and CTX and the documented electrostatic interaction between a potassium-selective channel and CTX that serves to insert the Lys-27 residue in CTX into the filter (58–60), we asked whether the same residue (Glu-40) that mediated the effect of imipramine was also responsible for the docking of the CTX on the surface of the PM. This is indeed the case as the E40A mutant was largely insensitive to CTX at 1 μM: γ is equal within error with or without CTX (75 ± 8 *versus* 78 ± 8 pS), and the P_o increased only modestly from 0.07 ± 0.04 without CTX to 0.11 ± 0.04 with CTX (Fig. 4*D* and Table 2).

Docking of CTX onto the extracellular surface of KvLm using a Rosetta docking protocol (61) that permits receptor and ligand flexibility provides clues to how CTX may stabilize the conductive conformation. The docking results can be grouped into two different KvLm-CTX binding models: one in which Glu-40 in the PM anchors the toxin by sequestering Lys-27 in CTX hovering over the filter (Fig. 4*E*) and a second in which the same lysine inserts its charge into S1 (Fig. 4*F*). In the first model, the toxin is anchored onto the PM extracellular surface through a network of hydrogen bonds (H–O distance, <2.2 Å) involving residues Arg-25, Lys-27, Ans-30, and Tyr-36 in CTX and residues Glu-40, Asp-46, and Asp-62 distributed among three subunits (B, C, and D) in the PM. In addition, the side chain of Glu-40 (Oϵ2) in subunit B of the PM, and Lys-27 (Nζ) in CTX form a salt bridge. In contrast, in the second model, there are no salt bridges formed between CTX and pore, and the toxin remains anchored through hydrogen bonds only to a single PM subunit. In comparison with the first model, two new hydrogen bonds are identified: one between the carbonyl oxygen of Tyr-60 and the side chain of Lys-27 (Nζ) in CTX and one between the side chain of Glu-40 (Oϵ1) and the backbone amide of Lys-31 (N) in CTX (H–O distance, 2.05 and 2.15 Å, respectively). This model is similar to that proposed for the interaction of CTX with Shaker and presumably represents a CTX-blocked permeation path. In Shaker, the position of Glu-40 is occupied by Phe-425 (Fig. 4*A*); the absence of a charge at this position may account for CTX block of Shaker.

Comparison of the first model for CTX binding (Fig. 4*E*) with the model proposed for imipramine binding reveals two commonalities: a dependence on Glu-40 and the positioning of a lid over the exit of the permeation path. We propose, therefore, that both gating modulators induce a stabilization of the conductive conformation through the same "lid mechanism," namely the channel filter gate covered by a lid.

Covalent Attachment of Fluorescein at a Cysteine Residue Selectively Introduced near the Filter Gate Stabilizes the Conductive Conformation of the Channel—To assess the validity of the postulated lid mechanism, we exploited the key role of Glu-40 as an anchoring site and replaced it by cysteine (E40C). We conjectured that the accessible Cys would allow reaction with fluorescein maleimide leading to the covalent attachment of the probe at a site that would promote its hovering over the filter gate and accordingly imitate the "lid" effect observed with imipramine and CTX (Fig. 5, *D* and *E*). As shown in Fig. 5*C*, this was indeed the case: for E40C, $\gamma = 80 \pm 7$ pS with a P_o of 0.06 ± 0.03 (Fig. 5*B* and Table 2); by contrast, for E40C-fluorescein, $\gamma = 7 \pm 1$ pS with a P_o of 0.74 ± 0.05 (Fig. 5*C* and Table 2) in fair agreement with the features resulting from the interaction with imipramine and CTX (Table 2). Therefore, we conclude that

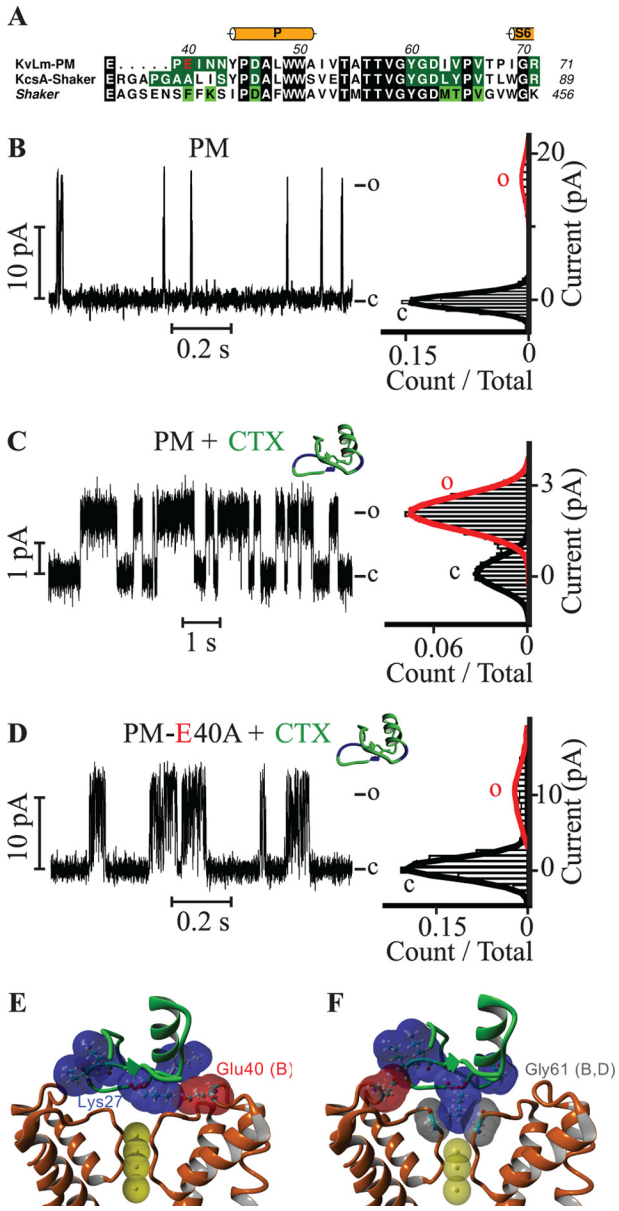

FIGURE 4. **The neurotoxin CTX gates the KvLm PM.** *A*, alignment of the TM5-TM6 extracellular linker sequences present in KvLm, in a KcsA mutant sensitive to CTX (KcsA-Shaker), and in Shaker (gi 92090610), a CTX-sensitive eukaryotic Kv channel pore. Conserved residues are shaded *black*. Glu-40 in KvLm is shown in *red*. Residues predicted by a structural model to contact (<4 Å) CTX in KvLm and in KcsA-Shaker (Protein Data Bank code 2A9H (42)) are shaded *dark green*. Residues that when mutated in Shaker alter the binding affinity by >50-fold are shaded *light green* (53). Single channel steady-state current records (*left*) of WT PM (*B* and *C*) and of the E40A mutant KvLm PM (*D*) and their corresponding normalized all-point histograms (*right*) in symmetric DOPA bilayers with 1 μM CTX in the *cis* droplet (*C* and *D*) are shown. *E* and *F*, side views of two fundamentally different models for the interaction between the KvLm PM filter gate and CTX (*green ribbon*) generated by docking experiments. The highest scoring model (*E*) shows the side chain of Glu-40 forming an electrostatic interaction with Lys-27 in CTX, and the fifth highest scoring model (*F*) depicts Lys-27 interacting with Gly-61 in the selectivity filter. CTX is colored *green* with lysine residues shown in surface-accessible representation colored *blue*. The surfaces of the PM residues Glu-40 (in *red*) and Gly-61 (in *gray*) interacting with CTX are shown. Subunits are indicated in *parentheses*. *c*, closed; *o*, open.

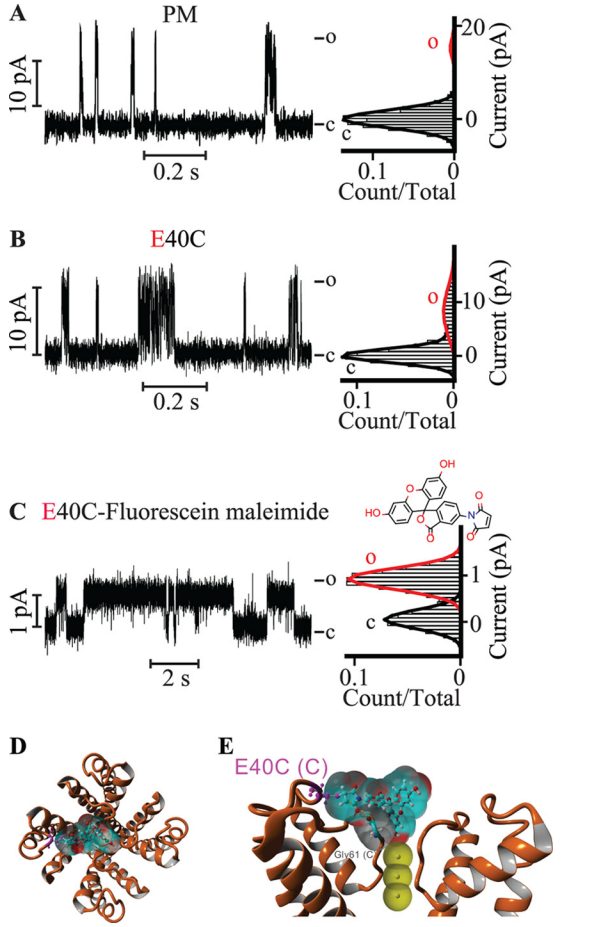

FIGURE 5. **Covalently attached fluorescein at Glu-40 gates the KvLm PM.** Single channel steady-state current records (*left*) and their corresponding normalized all-point histograms (*right*) of WT KvLm PM (*A*) and of the KvLm PM E40C mutant (*B* and *C*) reconstituted in symmetric DOPA bilayers before (*B*) and after (*C*) coupling with fluorescein 5-maleimide are shown. The structure of fluorescein 5-maleimide is shown above the current recording in *C*. *D*, extracellular view of a model for interaction of the coupled fluorescein 5-maleimide with the filter gate of KvLm PM (see "Experimental Procedures"). The channel PM is depicted in *orange ribbons* (Protein Data Bank code 4H33). *E*, side view of two opposing subunits. The solvent-accessible surfaces of the interacting residues in the PM are shown and are color-coded according to charge (*red* for Glu-40 and Asp-62 and *gray* for Gly-61). *Yellow dashed lines* show hydrogen bond sites. Residues are labeled with subunit in *parentheses*. The solvent-accessible surface of fluorescein is depicted in *light blue*. K^+ ions at positions S2, S3, and S4 in the filter are depicted as *solid yellow spheres* displaying their accessible surface. *c*, closed; *o*, open.

the stabilization of these three distinct modulators plausibly proceeds by the postulated lid mechanism that prolongs the residence time of cargo at the filter gate.

Do Imipramine and CTX Have an Effect on the PM When All Four Voltage Sensors Are Present?—We have demonstrated previously that the pore in KvLm is a structural domain and a functional module (5, 36). To further test this notion, we asked whether the pore structural domain is a functional module in the context of the FL protein. If so, the effect of imipramine and CTX observed on the PM alone should be mostly reproduced in the FL when the PM is interacting with the voltage sensor modules. As shown in Fig. 6, the PM is indeed a functional module: for the FL KvLm, 5 μM imipramine (Fig. 6*B*) and 1 μM CTX (Fig. 6*C*) increased the open probability by an average of >10-fold from 0.07 ± 0.01 to 0.74 ± 0.08 (Table 1) while significantly decreasing γ from 70 ± 3 to 16 ± 2 pS when 5 μM imipramine bathed the selectivity filter and to 14 ± 3 pS when 1 μM CTX was latched onto the extracellular surface of the PM. From

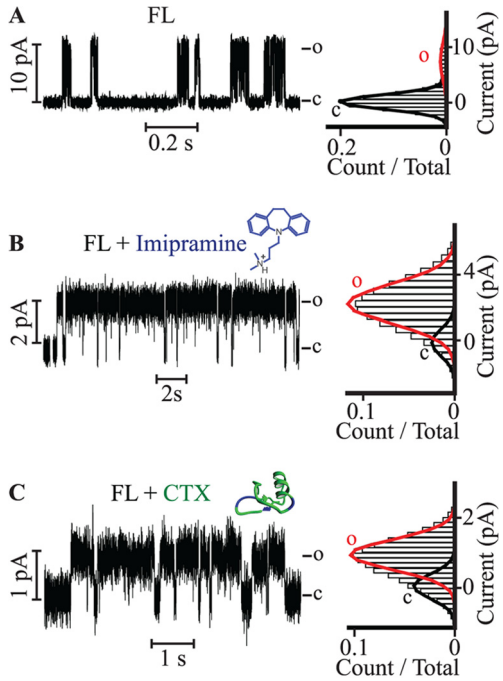

FIGURE 6. **Imipramine and CTX gate the PM in the presence of all sensors (FL).** Steady-state single channel current records (*left*) of KvLm FL reconstituted in a DOPA lipid bilayer (*A*), in presence of 5 μM imipramine (*B*), and in the presence of 1 μM CTX (*C*) at the filter gate (*cis* droplet). The corresponding normalized all-point histograms are shown in the *right-hand column*. *c*, closed; *o*, open.

these results, we conclude that 1) the PM alone is a faithful structural target for the development of drugs that bind to PM in the full-length channel, 2) the low open probability observed for the PM and FL at activating potentials is a property of the pore and not of the sensor, and 3) the likely source for the low open probability in both cases is an unstable filter gate.

DISCUSSION

Here we demonstrate that the premature closing of KvLm responsible for its short residence in the open state at saturating activating potentials may be overcome by an association of the inactivation gate of the pore located at the selectivity filter with imipramine or CTX and that this modulation is faithfully mimicked by the covalent attachment of fluorescein at an anchor site near the filter gate. We show that all three gating stabilizers achieve this effect at the expense of a reduction in outward conductance. The results highlight two fundamental properties of the selectivity filter gate in a Kv channel. 1) The structural plasticity of the filter (33) makes it sensitive to its environment, and 2) the stability of the open conductive conformation is dictated by the residence time of a permeant ion (or water) at the filter.

We propose that imipramine, CTX, and attached fluorescein act as a lid covering the permeation exit. Given that the covalent attachment of a lid to the cysteine mutant of Glu-40 reproduced the effect of the other two modulators, we surmise that a direct interaction underlies the observed effect. This does not exclude a contribution of an indirect interaction between partners to the observable effect. In both interaction modes, the reduction in outward flux, presumably resulting from a steric hindrance at the exit from the filter, is shown to stabilize the conductive conformation of the channel: by delaying the exit of K^+ or water from the filter, these modulators increase their residence time within the filter. It is this longer embrace between "cargo" and gate that we surmise accounts for the stabilization of the conductive conformation. This novel lid mechanism is similar to that proposed for the interaction of the filter gate of Kv channels with Rb^+: reduction in conductance, prolongation of the open time, and ablation of inactivation resulting from an increased residence time of the permeating ion at the gate (25, 26, 36, 47, 62–64) collectively support the "foot-in-the-door" mechanism elegantly put forth by Armstrong and colleague (25). There is nonetheless a salient difference between the newly proposed lid mechanism and that advanced by Armstrong and colleague (25): in the lid mechanism, the "foot in the door" has moved away from the door and been replaced by a lid (body) right outside the door. There is little contact between gating modifier and gate. However, from a distance, CTX and imipramine produce the same end effect postulated by the foot-in-the-door mechanism: prolonged occupancy of the ion binding sites at the filter gate. In addition, the proposed lid mechanism is complementary to the "ion depletion of the pore" hypothesis previously postulated to give rise to flickering and instability of the conductive conformation of the filter gate of other K^+ channels (24, 41, 65, 66). As presented, the model implies that the filter gate transits between conductive and nonconductive conformations and that the conformation of the gate depends stringently on the occupancy of the filter by either water or a permeant ion (24).

The ability to convert a pore that opens only briefly, alone, or in the context of the full-length protein to a pore that remains open more than 50% of the time at activating potentials indicates first that the transition from nonconductive to conductive conformation in the KvLm PM requires little energy once the sensors have moved to their activated position. This is in good agreement with the results from two previous studies on KvLm that established that 1) the PM can gate open long enough in the absence of any potential to allow TBA to enter and block the channel (5) and 2) the frequency with which the PM opens is not significantly different from the frequency with which the full-length channel opens (37). Collectively, the body of work on KvLm thus far posits that the primary role of the sensor is to mechanically lock closed the channel at nonactivating potentials, thereby insulating the gating machinery from spurious activators present in the extracellular medium or in the membrane (67, 68). Second, the sensitivity of both PM and FL to the identified gating stabilizers suggests that the activation process of Kv channels is vulnerable to the demands of their surroundings at the kinetic step when the sensor has lost control of its covalently attached PM: the step preceding onset of conduction when the sensor has moved but the pore is not yet conducting (14, 69–73). It is in this brief instant that the closed and open conformations of the pore become most energetically similar and therefore easily forced in one direction or the other that the modulators override the control of the sensor on the filter gate of the pore. Therefore, we predict that the mechanism here proposed may be applicable to the interaction of other Kv chan-

nels with gating modulators that promote a long lasting relation between filter gate and cargo.

REFERENCES

1. MacKinnon, R. (1991) Determination of the subunit stoichiometry of a voltage-activated potassium channel. *Nature* **350,** 232–235
2. Jiang, Y., Lee, A., Chen, J., Ruta, V., Cadene, M., Chait, B. T., and MacKinnon, R. (2003) X-ray structure of a voltage-dependent K^+ channel. *Nature* **423,** 33–41
3. Long, S. B., Campbell, E. B., and Mackinnon, R. (2005) Crystal structure of a mammalian voltage-dependent Shaker family K^+ channel. *Science* **309,** 897–903
4. Long, S. B., Tao, X., Campbell, E. B., and MacKinnon, R. (2007) Atomic structure of a voltage-dependent K^+ channel in a lipid membrane-like environment. *Nature* **450,** 376–382
5. Santos, J. S., Asmar-Rovira, G. A., Han, G. W., Liu, W., Syeda, R., Cherezov, V., Baker, K. A., Stevens, R. C., and Montal, M. (2012) Crystal structure of a voltage-gated K^+ channel pore module in a closed state in lipid membranes. *J. Biol. Chem.* **287,** 43063–43070
6. Long, S. B., Campbell, E. B., and Mackinnon, R. (2005) Voltage sensor of Kv1.2: structural basis of electromechanical coupling. *Science* **309,** 903–908
7. Bezanilla, F. (2000) The voltage sensor in voltage-dependent ion channels. *Physiol. Rev.* **80,** 555–592
8. Liu, Y., Holmgren, M., Jurman, M. E., and Yellen, G. (1997) Gated access to the pore of a voltage-dependent K^+ channel. *Neuron* **19,** 175–184
9. Hoshi, T., Zagotta, W. N., and Aldrich, R. W. (1991) Two types of inactivation in Shaker K^+ channels: effects of alterations in the carboxy-terminal region. *Neuron* **7,** 547–556
10. Choi, K. L., Aldrich, R. W., and Yellen, G. (1991) Tetraethylammonium blockade distinguishes two inactivation mechanisms in voltage-activated K^+ channels. *Proc. Natl. Acad. Sci. U.S.A.* **88,** 5092–5095
11. Liu, Y., Jurman, M. E., and Yellen, G. (1996) Dynamic rearrangement of the outer mouth of a K^+ channel during gating. *Neuron* **16,** 859–867
12. Hodgkin, A. L., and Huxley, A. F. (1952) A quantitative description of membrane current and its application to conduction and excitation in nerve. *J. Physiol.* **117,** 500–544
13. Islas, L. D., and Sigworth, F. J. (1999) Voltage sensitivity and gating charge in Shaker and Shab family potassium channels. *J. Gen. Physiol.* **114,** 723–742
14. Pathak, M., Kurtz, L., Tombola, F., and Isacoff, E. (2005) The cooperative voltage sensor motion that gates a potassium channel. *J. Gen. Physiol.* **125,** 57–69
15. Loots, E., and Isacoff, E. Y. (2000) Molecular coupling of S4 to a K^+ channel's slow inactivation gate. *J. Gen. Physiol.* **116,** 623–636
16. Vaid, M., Horne, A., Claydon, T., and Fedida, D. (2009) Rapid outer pore movements after opening in a KV1 potassium channel are revealed by TMRM fluorescence from the S3-S4 linker, and modulated by extracellular potassium. *Channels* **3,** 3–5
17. Lee, S. Y., Banerjee, A., and MacKinnon, R. (2009) Two separate interfaces between the voltage sensor and pore are required for the function of voltage-dependent K^+ channels. *PLoS Biol.* **7,** e47
18. Lainé, M., Lin, M. C., Bannister, J. P., Silverman, W. R., Mock, A. F., Roux, B., and Papazian, D. M. (2003) Atomic proximity between S4 segment and pore domain in Shaker potassium channels. *Neuron* **39,** 467–481
19. Hoshi, T., Zagotta, W. N., and Aldrich, R. W. (1990) Biophysical and molecular mechanisms of Shaker potassium channel inactivation. *Science* **250,** 533–538
20. Zagotta, W. N., Hoshi, T., and Aldrich, R. (1990) Restoration of inactivation in mutants of Shaker potassium channels by a peptide derived from ShB. *Science* **250,** 568–571
21. Ogielska, E. M., Zagotta, W. N., Hoshi, T., Heinemann, S. H., Haab, J., and Aldrich, R. W. (1995) Cooperative subunit interactions in C-type inactivation of K channels. *Biophys. J.* **69,** 2449–2457
22. Loots, E., and Isacoff, E. Y. (1998) Protein rearrangements underlying slow inactivation of the Shaker K^+ channel. *J. Gen. Physiol.* **112,** 377–389
23. Panyi, G., Sheng, Z., and Deutsch, C. (1995) C-type inactivation of a voltage-gated K^+ channel occurs by a cooperative mechanism. *Biophys. J.* **69,** 896–903
24. Bernèche, S., and Roux, B. (2005) A gate in the selectivity filter of potassium channels. *Structure* **13,** 591–600
25. Swenson, R. P., Jr., and Armstrong, C. M. (1981) K^+ channels close more slowly in the presence of external K^+ and Rb^+. *Nature* **291,** 427–429
26. Demo, S. D., and Yellen, G. (1991) The inactivation gate of the Shaker K^+ channel behaves like an open-channel blocker. *Neuron* **7,** 743–753
27. Pardo, L. A., Heinemann, S. H., Terlau, H., Ludewig, U., Lorra, C., Pongs, O., and Stühmer, W. (1992) Extracellular K^+ specifically modulates a rat brain K^+ channel. *Proc. Natl. Acad. Sci. U.S.A.* **89,** 2466–2470
28. Baukrowitz, T., and Yellen, G. (1995) Modulation of K^+ current by frequency and external $[K^+]$: a tale of two inactivation mechanisms. *Neuron* **15,** 951–960
29. Kiss, L., and Korn, S. (1998) Modulation of C-type inactivation by K^+ at the potassium channel selectivity filter. *Biophys. J.* **74,** 1840–1849
30. Ambriz-Rivas, M., Islas, L. D., and Gomez-Lagunas, F. (2005) K^+-dependent stability and ion conduction of Shab K^+ channels: a comparison with Shaker channels. *Pflugers Arch.* **450,** 255–261
31. Grissmer, S., and Cahalan, M. (1989) TEA prevents inactivation while blocking open K^+ channels in human T lymphocytes. *Biophys. J.* **55,** 203–206
32. Koch, E. D., Olivera, B. M., Terlau, H., and Conti, F. (2004) The binding of κ-conotoxin PVIIA and fast C-type inactivation of Shaker K^+ channels are mutually exclusive. *Biophys. J.* **86,** 191–209
33. Noskov, S. Y., Bernèche, S., and Roux, B. (2004) Control of ion selectivity in potassium channels by electrostatic and dynamic properties of carbonyl ligands. *Nature* **431,** 830–834
34. Santos, J. S., Lundby, A., Zazueta, C., and Montal, M. (2006) Molecular template for a voltage sensor in a novel K^+ channel. I. Identification and functional characterization of KvLm, a voltage-gated K^+ channel from *Listeria monocytogenes*. *J. Gen. Physiol.* **128,** 283–292
35. Lundby, A., Santos, J. S., Zazueta, C., and Montal, M. (2006) Molecular template for a voltage sensor in a novel K^+ channel. II. Conservation of a eukaryotic sensor fold in a prokaryotic K^+ channel. *J. Gen. Physiol.* **128,** 293–300
36. Santos, J. S., Grigoriev, S. M., and Montal, M. (2008) Molecular template for a voltage sensor in a novel K^+ channel. III. Functional reconstitution of a sensorless pore module from a prokaryotic Kv channel. *J. Gen. Physiol.* **132,** 651–666
37. Syeda, R., Santos, J. S., Montal, M., and Bayley, H. (2012) Tetrameric assembly of KvLm K^+ channels with defined numbers of voltage sensors. *Proc. Natl. Acad. Sci. U.S.A.* **109,** 16917–16922
38. Qin, F. (2004) Restoration of single-channel currents using the segmental k-means method based on hidden Markov modeling. *Biophys. J.* **86,** 1488–1501
39. Morris, G. M., Huey, R., Lindstrom, W., Sanner, M. F., Belew, R. K., Goodsell, D. S., and Olson, A. J. (2009) AutoDock4 and AutoDockTools4: automated docking with selective receptor flexibility. *J. Comput. Chem.* **30,** 2785–2791
40. Duan, Y., Wu, C., Chowdhury, S., Lee, M. C., Xiong, G., Zhang, W., Yang, R., Cieplak, P., Luo, R., Lee, T., Caldwell, J., Wang, J., and Kollman, P. (2003) A point-charge force field for molecular mechanics simulations of proteins based on condensed-phase quantum mechanical calculations. *J. Comput. Chem.* **24,** 1999–2012
41. Zhou, Y., Morais-Cabral, J. H., Kaufman, A., and MacKinnon, R. (2001) Chemistry of ion coordination and hydration revealed by a K^+ channel-Fab complex at 2.0 Å resolution. *Nature* **414,** 43–48
42. Yu, L., Sun, C., Song, D., Shen, J., and Xu, N. (2005) Nuclear magnetic resonance structural studies of a potassium channel-charybdotoxin complex. *Biochemistry* **44,** 15834–15841
43. Bayley, H., Cronin, B., Heron, A., Holden, M. A., Hwang, W. L., Syeda, R., Thompson, J., and Wallace, M. (2008) Droplet interface bilayers. *Mol. BioSyst.* **4,** 1191–1208
44. French, R. J., and Shoukimas, J. J. (1981) Blockage of squid axon potassium conductance by internal tetra-*N*-alkylammonium ions of various sizes. *Biophys. J.* **34,** 271–291
45. Yohannan, S., Hu, Y., and Zhou, Y. (2007) Crystallographic study of the

tetrabutylammonium block to the KcsA K^+ channel. *J. Mol. Biol.* **366,** 806–814
46. Santos, J. S., Lee, D.-K., and Ramamoorthy, A. (2004) Effects of antidepressants on the conformation of phospholipid headgroups studied by solid-state NMR. *Magn. Reson. Chem.* **42,** 105–114
47. Zhou, Y., and MacKinnon, R. (2003) The occupancy of ions in the K^+ selectivity filter: charge balance and coupling of ion binding to a protein conformational change underlie high conduction rates. *J. Mol. Biol.* **333,** 965–975
48. Aqvist, J., and Luzhkov, V. (2000) Ion permeation mechanism of the potassium channel. *Nature* **404,** 881–884
49. Morais-Cabral, J. H., Zhou, Y., and MacKinnon, R. (2001) Energetic optimization of ion conduction rate by the K^+ selectivity filter. *Nature* **414,** 37–42
50. Bernèche, S., and Roux, B. (2001) Energetics of ion conduction through the K^+ channel. *Nature* **414,** 73–77
51. Park, C. S., and Miller, C. (1992) Interaction of charybdotoxin with permeant ions inside the pore of a K^+ channel. *Neuron* **9,** 307–313
52. Miller, C. (1995) The charybdotoxin family of K^+ channel-blocking peptides. *Neuron* **15,** 5–10
53. Goldstein, S. A., Pheasant, D. J., and Miller, C. (1994) The charybdotoxin receptor of a Shaker K^+ channel: peptide and channel residues mediating molecular recognition. *Neuron* **12,** 1377–1388
54. Naranjo, D., and Miller, C. (1996) A strongly interacting pair of residues on the contact surface of charybdotoxin and a Shaker K^+ channel. *Neuron* **16,** 123–130
55. MacKinnon, R., Reinhart, P. H., and White, M. M. (1988) Charybdotoxin block of Shaker K^+ channels suggests that different types of K^+ channels share common structural features. *Neuron* **1,** 997–1001
56. Goldstein, S. A., and Miller, C. (1992) A point mutation in a Shaker K^+ channel changes its charybdotoxin binding site from low to high affinity. *Biophys. J.* **62,** 5–7
57. MacKinnon, R., and Miller, C. (1989) Mutant potassium channels with altered binding of charybdotoxin, a pore-blocking peptide inhibitor. *Science* **245,** 1382–1385
58. Park, C. S., and Miller, C. (1992) Mapping function to structure in a channel-blocking peptide: electrostatic mutants of charybdotoxin. *Biochemistry* **31,** 7749–7755
59. Stocker, M., and Miller, C. (1994) Electrostatic distance geometry in a K^+ channel vestibule. *Proc. Natl. Acad. Sci. U.S.A.* **91,** 9509–9513
60. Thompson, J., and Begenisich, T. (2000) Electrostatic interaction between charybdotoxin and a tetrameric mutant of Shaker K^+ channels. *Biophys. J.* **78,** 2382–2391
61. Lyskov, S., and Gray, J. J. (2008) The RosettaDock server for local protein-protein docking. *Nucleic Acids Res.* **36,** W233–W238
62. Seebohm, G., Sanguinetti, M. C., and Pusch, M. (2003) Tight coupling of rubidium conductance and inactivation in human KCNQ1 potassium channels. *J. Physiol.* **552,** 369–378
63. Shahidullah, M., and Covarrubias, M. (2003) The link between ion permeation and inactivation gating of Kv4 potassium channels. *Biophys. J.* **84,** 928–941
64. Matteson, D. R., and Swenson, R. P. (1986) External monovalent cations that impede the closing of K channels. *J. Gen. Physiol.* **87,** 795–816
65. Schroeder, I., and Hansen, U. P. (2007) Saturation and microsecond gating of current indicate depletion-induced instability of the MaxiK selectivity filter. *J. Gen. Physiol.* **130,** 83–97
66. Abenavoli, A., DiFrancesco, M. L., Schroeder, I., Epimashko, S., Gazzarrini, S., Hansen, U. P., Thiel, G., and Moroni, A. (2009) Fast and slow gating are inherent properties of the pore module of the K^+ channel Kcv. *J. Gen. Physiol.* **134,** 219–229
67. Patlak, J. B. (1999) Cooperating to unlock the voltage-dependent K channel. *J. Gen. Physiol.* **113,** 385–388
68. Armstrong, C. M. (2003) Voltage-gated K channels. *Sci. STKE* **2003,** re10
69. Schmidt, D., del Mármol, J., and MacKinnon, R. (2012) Mechanistic basis for low threshold mechanosensitivity in voltage-dependent K^+ channels. *Proc. Natl. Acad. Sci. U.S.A.* **109,** 10352–10357
70. del Camino, D., Kanevsky, M., and Yellen, G. (2005) Status of the intracellular gate in the activated-not-open state of shaker K^+ channels. *J. Gen. Physiol.* **126,** 419–428
71. Schoppa, N. E., and Sigworth, F. J. (1998) Activation of shaker potassium channels. I. Characterization of voltage-dependent transitions. *J. Gen. Physiol.* **111,** 271–294
72. Zagotta, W. N., Hoshi, T., Dittman, J., and Aldrich, R. W. (1994) Shaker potassium channel gating. II: transitions in the activation pathway. *J. Gen. Physiol.* **103,** 279–319
73. Loboda, A., and Armstrong, C. M. (2001) Resolving the gating charge movement associated with late transitions in K channel activation. *Biophys. J.* **81,** 905–916